

1
2
3
4
5
6
7
8
9

Functional integration of “undead” neurons in the olfactory system

10 Lucia L. Prieto-Godino^{1,#,+}, Ana F. Silbering^{1,#}, Mohammed A. Khallaf^{2,‡}, Steeve
11 Cruchet^{1,‡}, Karolina Bojkowska³, Sylvain Pradervand^{3,4}, Bill S. Hansson², Markus
12 Knaden² and Richard Benton^{1,*}

13
14
15
16
17
18
19

¹Center for Integrative Genomics
Faculty of Biology and Medicine
University of Lausanne
CH-1015 Lausanne
Switzerland

20
21
22
23
24

²Department of Evolutionary Neuroethology
Max Planck Institute for Chemical Ecology
D-07745 Jena
Germany

25
26
27
28
29
30

³Genomic Technologies Facility
Faculty of Biology and Medicine
University of Lausanne
CH-1015 Lausanne
Switzerland

31
32
33
34
35

⁴Vital-IT Group, SIB
Swiss Institute of Bioinformatics
CH-1015 Lausanne
Switzerland

36
37
38
39
40

⁺Present address: The Francis Crick Institute, 1 Brill Place, London, NW1 1BF,
United Kingdom

41
42
43
44

[#]These authors contributed equally to this work
[‡]These authors contributed equally to this work

45
46
47
48
49

*Corresponding author:

T: ++41 21 692 3932
E: Richard.Benton@unil.ch

50 Summary

51 Programmed cell death (PCD) is widespread during nervous system
52 development, eliminating up to half of the neurons in certain regions of
53 mammalian brains^{1,2}. PCD can serve to counterbalance the surpluses of neural
54 production, and contribute to the formation of correct connectivity³⁻⁶. Here we
55 show that cells normally fated to die also represent a reservoir of potential
56 neurons that could contribute to neural circuit evolution. We used as a model the
57 *Drosophila* peripheral olfactory system, whose lineages exhibit extensive,
58 stereotyped patterns of PCD⁷⁻¹⁰. Inhibition of developmental PCD is sufficient to
59 generate many new cells in the antenna that express neural markers.
60 Electrophysiological recordings from these “undead” neurons’ sensory dendrites
61 reveal that they exhibit basal and odour-evoked activity similar to wild-type
62 neurons. Transcriptomic and *in situ* analyses demonstrate that undead antennal
63 neurons express a subset of olfactory receptor genes, including those expressed
64 naturally in other olfactory organs in adults and larvae. Intriguingly, this subset is
65 enriched for relatively young gene duplicates that are normally co-expressed in
66 wild-type neurons. Undead neurons therefore provide a potential cellular
67 substrate to allow the switch of receptors between sensory organs or life stages,
68 as well as accommodate recently-generated receptor genes. Finally, we show
69 that undead neurons can extend axons to novel regions in the primary olfactory
70 centre in the brain, where they may form synaptic connections with second order
71 projection neurons. These data indicate that undead neurons retain a molecular
72 programme that enables their functional integration into the extant olfactory
73 system, raising the possibility that alterations in PCD patterning during evolution
74 is a simple way to generate new sensory pathways. Consistently, comparative
75 analysis of homologous olfactory lineages across the drosophilid phylogeny
76 revealed multiple independent examples where the presence of an additional
77 neuron is consistent with evolutionary fate changes from PCD to a functional
78 olfactory sensory neuron.

79
80 A fundamental way in which nervous systems evolve is through increases in the
81 numbers of neurons¹¹⁻¹³. Additional sensory neurons can enable higher sensitivity
82 to environmental signals or lead to functional diversification to support acquisition
83 of novel detection abilities. Increases in central neuron number might underlie
84 diverse enhancements in cognitive abilities¹⁴, such as parallel processing and
85 memory storage. The generation of more neurons could be achieved through
86 greater production during development – by increasing the number and/or
87 proliferation of neural precursor cells – a process that appears to underlie
88 neocortical expansion during primate evolution¹⁵. Alternatively (or additionally),
89 given the widespread occurrence of programmed cell death (PCD) during neural
90 development^{1,2}, prevention of this process can potentially yield a pool of
91 additional neurons. Consistent with this idea, genetic blockage of PCD in mice or
92 *D. melanogaster* results in the development of enlarged, albeit malformed,
93 nervous systems^{16,17}. Moreover, in *C. elegans*, the function of an experimentally-
94 ablated pharyngeal neuron can be partially compensated by a sister cell rescued
95 from PCD by a caspase mutation¹⁸.

96 Here we examined the potential of PCD blockage in the formation of novel
97 neural pathways in the *D. melanogaster* olfactory system. This model is of
98 interest because its development involves prevalent PCD and its molecular

99 neuroanatomy is well-described. The principal olfactory organ, the third antennal
100 segment, is covered with ~400 porous sensory hairs (sensilla) of morphologically-
101 diverse classes (Fig. 1a)¹⁹. An individual sensillum derives from a single sensory
102 organ precursor (SOP) cell that is specified in the antennal imaginal disc^{20,21}.
103 Each SOP gives rise to a short, fixed lineage of asymmetric cell divisions that
104 produces eight terminal cells with distinct identities^{8,21} (Fig. 1b). Four adopt non-
105 neural (“support cell”) fates, and are involved in the construction of the hair,
106 amongst other roles. The other four cells can potentially differentiate as olfactory
107 sensory neurons (OSNs), which express a single (or rarely two) sensory receptor
108 genes, develop ciliated dendrites that innervate the lumen of the sensillum hair,
109 and project axons towards a specific glomerulus in the primary olfactory centre in
110 the brain (antennal lobe).

111 There are ~20 sensillum classes, housing stereotyped combinations of
112 OSNs (Extended Data Table 1)²²⁻²⁴. Of these, only one class (antennal basiconic
113 1 [ab1]) contains four neurons, with the others containing fewer – mostly two or
114 three – OSNs. The “missing” neurons are removed by PCD ~22-32 hours after
115 puparium formation (APF)⁷⁻¹⁰, when OSN terminal fate is established²⁵.

116 To block PCD during OSN development, we first used animals bearing
117 deletions in the tandem cluster of pro-apoptotic genes (*head involution defective*
118 (*hid*), *grim*, *reaper* (*rpr*) and *sickle* (*skl*)), which encode transcription factors critical
119 for promoting developmentally-regulated PCD in diverse tissues (Fig. 1c)^{4,26}.
120 Homozygous chromosomal deficiencies that span the entire cluster cause
121 embryonic lethality. However, a trans-heterozygous combination
122 (*Df(3L)H99/Df(3L)XR38*), which removes both copies of *rpr*, and one copy each of
123 *hid*, *grim* and *skl*, allowed recovery of a few viable adults. Immunofluorescence on
124 whole-mount antennae with an antibody against the neural nuclear marker, Elav,
125 revealed a clear increase in the number of labelled cells in mutant animals
126 compared to controls (Fig. 1d), indicating that new neurons form when cell death
127 is prevented.

128 PCD might be impaired in these mutants at any stage of olfactory system
129 development, including during SOP specification. To selectively block the terminal
130 PCD of OSN lineages (Fig. 1b), we down-regulated expression of *hid*, *grim* and
131 *rpr* by transgenic RNAi from ~18 h APF using the *pebbled-Gal4* (*peb-Gal4*) driver,
132 which is broadly-expressed in post-mitotic terminal OSN precursors²⁷. Blockage
133 of OSN-specific PCD in this manner also led to a significant increase in Elav-
134 positive cells (Fig. 1e). The number of extra Elav-positive cells observed in these
135 experiments (~200-300, recognising the limits of automated neuron counting in
136 nuclei-dense tissue (Extended Data Fig. 1)) is in line with estimates of the total
137 number of potential undead neurons (~300-400) (Extended Data Table 1). We
138 further confirmed the role of the PCD pathway in the antenna through expression
139 of the baculoviral caspase inhibitor p35²⁸ with the same driver. *peb-Gal4>UAS-*
140 *p35* (hereafter “PCD-blocked”) animals displayed higher numbers of Elav-positive
141 cells compared to a *peb-Gal4* (control) (Fig. 1f), consistent with a caspase-
142 dependent PCD pathway in this sensory organ.

143 To determine whether these additional Elav-positive cells are functional
144 neurons, we performed single-sensillum electrophysiological recordings. We
145 focused on one class of trichoid sensilla, at1, which houses a single OSN in
146 wildtype animals, due to PCD of the other three potential neurons in the lineage⁹.
147 This OSN expresses OR67d, a receptor for the pheromone *11-cis-vaccenyl*
148 acetate (cVA)²⁹. at1 sensilla are easily recognised by their sparse basal

149 (spontaneous) pattern of spikes of a single amplitude, and the robust train of
150 spikes that occur only upon cVA presentation (Fig. 2a,d). In PCD-blocked
151 animals, these sensilla often contain additional spikes of smaller amplitude (Fig.
152 2b-c), suggesting the presence of one or more extra, active OSNs (spike
153 amplitude is defined by the OSN not the receptor gene³⁰). Moreover, exposure to
154 a blend of food-derived odours (which activate many different ORs³¹) led to
155 responses of the undead neurons in about one-third of the tested sensilla (Fig.
156 2d-e); the non-responding undead neurons may express receptors activated by
157 other stimuli. These observations indicate that blocking PCD can lead to the
158 development of functional OSNs. The variable odour-evoked responses of these
159 undead neurons to food-derived odours (Fig. 2e) suggests that these cells do not
160 have a fixed identity in at1 sensilla but rather express one of several different
161 types of receptors.

162 To identify the receptor genes expressed by undead OSNs, we performed
163 comparative transcriptomics of whole antennae of control and PCD-blocked
164 animals by RNA-sequencing. As a positive control, we first examined the changes
165 in transcript levels of *grim*, *rpr*, *hid* and *skl*, reasoning that inhibition of PCD
166 downstream in the pathway should lead to the presence of undead cells
167 expressing mRNAs for these pro-apoptotic genes (Fig. 1c). Indeed, three of these
168 genes showed higher expression levels in PCD-blocked antennae (Fig. 3a).

169 We next queried the transcript levels for all chemosensory receptors,
170 comprising *Odorant receptor (Or)*, *Ionotropic receptor (Ir)* and *Gustatory receptor*
171 (*Gr*) gene families (Extended Data Tables 1-2). Of the receptors previously
172 detected in antennal neurons *in situ*^{22,23,32}, we found that 10/36 *Ors*, 1/17 *Irs* and
173 0/3 *Grs* displayed a >1.5-fold increase in expression, suggesting that only
174 subsets of these receptors are expressed in the undead neurons (Fig. 3a-b and
175 Extended Data Tables 2-3).

176 To validate these transcriptomic data, we visualised the neuronal
177 expression of several of the *Ors in situ*. Transcripts for all of those tested by RNA
178 fluorescent *in situ* hybridisation (FISH) were detected in more neurons in PCD-
179 blocked antennae compared to controls (Fig. 3c and Extended Data Fig. 2a). In
180 some cases, these neurons were found only within the same region of the
181 antenna as the endogenous OSNs (e.g., *Or42b*, *Or65a*) while in others (e.g.,
182 *Or19a*, *Or43a*) undead neurons were observed in novel locations (Fig. 3c and
183 Extended Data Fig. 2b).

184 Notably, many of the other receptors displaying increases in transcript
185 levels normally act in other chemosensory organs, including one *Or* expressed in
186 the maxillary palp (*Or85e*), two larval *Ors*, and seven *Gr* genes, which function in
187 various gustatory organs (Fig. 2a and Extended Data Tables 2-3). *In situ* analysis
188 revealed the presence of transcripts for *Or85e* and the larval-specific *Or33b* in
189 populations of undead neurons in PCD-blocked antennae (Fig. 3d).

190 Beyond these cases, the RNA levels of the vast majority of receptor genes
191 were either unchanged or slightly down-regulated in PCD-blocked antennae (Fig.
192 3a and Extended Data Table 2). Consistently, *in situ* analysis of a sample of
193 antennal genes revealed only a very small increase (e.g., *Ir75c*), no change (e.g.,
194 *Or13a*, *Or67d*, *Ir75b*), or a decrease (e.g., *Or35a*, *Or22a*) in the size of the
195 corresponding neuron populations (Fig. 3e, and Extended Data Fig. 2c). The
196 latter, unexpected phenotype raises the possibility that undead neurons impact
197 (directly or indirectly) the specification and/or survival of certain populations of
198 neurons.

199 What properties characterise the small subset of receptors that are
200 expressed in undead neurons? They are normally expressed in neurons housed
201 in diverse sensillum types: basiconic (e.g., *Or42b*), trichoid (e.g., *Or65a*),
202 intermediate (e.g., *Or19a*), and coeloconic (e.g., *Ir75d*) (Fig. 3b). By contrast,
203 most of these receptors (including 9/10 *Ors*) are activated in OSNs derived from
204 the Nba precursor cell; the remaining *Or* (*Or43a*) and the sole *Ir* (*Ir75d*) are
205 expressed in Naa-derived OSNs (Fig. 1b and Extended Data Table 3). This
206 pattern suggests that undead neurons (which are largely Naa-derived (Fig. 1b)
207 preserve gene-regulatory networks that are more similar to Nba/Naa cells than
208 Nab cells, perhaps reflecting the shared Notch activity in Naa and Nba precursors
209 (Fig. 1b)²¹. Finally, of the 13 *Ors* detected in undead neurons (including those
210 from other olfactory organs), ten are normally co-expressed with other *Or* genes,
211 a striking enrichment given the rarity of receptor co-expression within this
212 repertoire^{22,32}. While some co-expressed receptors remain co-expressed in
213 undead OSNs (e.g., *Or65a* and *Or65b* (Extended Data Fig. 2d)), this is not
214 always the case. For example, *Or19a*, but not the co-expressed *Or19b*, displays
215 up-regulation by RNA-seq (Extended Data Table 2). In addition, *in situ* analysis of
216 *Or49a* (using an *Or49a*-CD8:GFP (*Or49a*-GFP) reporter²²) and *Or85f*, reveals
217 that while these are always co-expressed in control antennal OSNs, in PCD-
218 blocked antennae there is a novel population of undead neurons that expresses
219 *Or49a*-GFP, but not *Or85f* (Fig. 3f).

220 We next investigated whether undead OSNs project their axons to the
221 antennal lobe. To label these neurons, we used an EGFP gene trap allele of *grim*
222 (*grim*^{M103811(EGFP)}), in which the fluorophore should report on the expression
223 pattern of this pro-apoptotic gene. In controls, *grim*^{M103811(EGFP)} expression is
224 detected only at background levels across the antenna; this is expected, as cells
225 that induce *grim* (and so EGFP) expression are fated to die (Fig. 4a). By contrast,
226 in PCD-blocked antennae, EGFP was detected in many soma (Fig. 4a), which
227 presumably represent the undead neurons previously observed with Elav
228 antibodies (Fig. 1f). In the brains of these animals, we observed that the EGFP-
229 labelled neurons innervate multiple glomeruli of the antennal lobe, indicating that
230 undead neurons can form axonal projections to the primary olfactory centre.
231 Antennal deafferentation experiments confirmed that the specific glomerular
232 signals in PCD-blocked animals were entirely due to the contribution of OSNs
233 (Fig. 4b).

234 Although the global architecture of the antennal lobe, as visualised by the
235 synaptic marker nc82 (Bruchpilot), is similar in control and PCD-blocked animals,
236 we did detect minor, and somewhat variable, morphological differences, including
237 less distinct boundaries between certain glomeruli and apparently novel regions
238 of neuropil. We wondered whether these differences reflect the innervation
239 patterns of populations of undead OSNs. To test this possibility, we examined the
240 projections of the neurons expressing the *Or49a*-GFP reporter, which labels
241 many more neurons in PCD-blocked antennae; some of these are different from
242 control neurons as they do not co-express *Or85f* (Fig. 3f). In control animals,
243 these neurons project to a single glomerulus, DL4, as previously described²². In
244 PCD-blocked animals, labelled axons projected to DL4, as well as to a second,
245 more anterior, glomerulus-like structure (Fig. 4c), which presumably correspond
246 to the wild-type *Or49a* neuron population and the undead neurons that express
247 this reporter, respectively (Fig. 3f). This observation suggests that undead
248 neurons can acquire distinct fates from control neurons, both by expressing

249 distinct receptor combinations and by forming different glomerular targets in the
250 brain.

251 We next asked whether such novel OSN axons can potentially synapse
252 with second-order projection neurons (PN). We combined the *Or49a*-GFP
253 reporter with a genetic driver for the majority of PNs (*GH146-QF>QUAS-Tomato*)
254 in control and antennal PCD-blocked flies. GH146-labelled processes were
255 detected in the novel *Or49a*-GFP-labelled glomerulus (Fig. 4d). Moreover, nc82
256 immunoreactivity, which reflects the presence of the active zone scaffolding
257 protein Bruchpilot³³ was also detected in this region (Fig. 4c), implying the
258 formation of synapses between OSNs and these second order neurons. The
259 novel connectivity does not result from the production of additional PNs (Fig. 4e),
260 suggesting that there is no mechanism to match OSN and PN numbers.

261 Our demonstration that inhibition of PCD is sufficient to allow the
262 development of new functional OSN populations that integrate into the olfactory
263 circuitry is consistent with the hypothesis that modulation of cell death patterns
264 during evolution can be a mechanism to create (or, conversely, remove) olfactory
265 channels. While the variation in OSN number per sensilla within *D. melanogaster*
266 implies that different SOP lineages have distinct regulation of PCD, we wondered
267 whether we could identify examples of divergent PCD patterning across shorter
268 evolutionary timescales by comparing homologous sensilla in different
269 drosophilids. Previous cross-species analyses suggested this is likely to be
270 relatively rare, as no differences in neuron numbers or pairing were reported in at
271 least a subset of basiconic and coeloconic sensilla in a limited range of
272 drosophilids (although receptor tuning properties do vary) (e.g.,³⁴⁻³⁶). We
273 therefore performed a broader electrophysiological screening of at1 sensilla in 24
274 drosophilid species. While the at1 sensilla of most species house a single cVA-
275 responsive neuron (Fig. 5a), similar to *D. melanogaster*, we identified several
276 species in which this sensillum houses two neurons of distinct spike amplitudes
277 (Fig. 5b), only one of which is cVA-responsive. The lack of genomic of these
278 species currently precludes further molecular analysis, although we assume that
279 cVA-responsive neurons express an OR67d orthologue and the partner neurons
280 a distinct OR of still-unknown sensory specificity. The at1 phenotype in these
281 species is reminiscent of that observed in *D. melanogaster* when PCD was
282 inhibited (Fig. 2) and provides natural examples of potential changes in PCD
283 patterns leading to novel neuronal circuit elements. Mapping the species whose
284 at1 sensilla house >1 OSN onto a phylogenetic tree, reveals that the acquisition
285 of an additional neuron has occurred independently multiple times during the
286 diversification of the drosophilid clade (Fig. 5c).

287 A future challenge will be to understand how PCD is determined in OSN
288 lineages and how these mechanisms relate to those defining the fate of the OSNs
289 that survive and express specific receptor genes. Our RNA-seq dataset provides
290 a molecular entry-point to answer these questions by identifying candidate genes
291 expressed highly in cells normally fated to die, similar to the pro-apoptotic factors.
292 Such knowledge is an essential pre-requisite to address how PCD pathways are
293 modified during evolution to selectively eliminate or create OSN populations.

294 One intriguing observation is that undead neuron populations do not
295 necessarily exhibit functional or anatomical properties that match those of existing
296 OSNs, for example, by expressing receptor genes not normally activated in
297 antennal neurons, or just one of two normally co-expressed receptors. These
298 traits presumably reflect properties of undead OSNs' "latent" gene regulatory

299 networks. Our work, together with a related study³⁷, reveals the outstanding
300 potential for modulation of cell death patterns to generate new neurons with
301 unique functions and wiring patterns.

302

303 **Acknowledgements**

304

305 We are grateful to I. Alali and M. Erdogmus for technical assistance, Darren
306 Williams and Sînziana Pop for sharing flies and discussions, Raquel Alvarez
307 Ocana for sharing information on OSN numbers, Mattias Alenius, the
308 Bloomington *Drosophila* Stock Center (NIH P40OD018537), and the
309 Developmental Studies Hybridoma Bank (NICHD of the NIH, University of Iowa)
310 for reagents. We thank Roman Arguello and members of the Benton laboratory
311 for comments on the manuscript. L.L.P.-G. was supported by a FEBS Long-Term
312 Fellowship. M.A.K., B.S.H., and M.K. are supported by the Max Planck Society.
313 Research in R.B.'s laboratory is supported by the University of Lausanne, an
314 ERC Consolidator Grant (615094) and the Swiss National Science Foundation.

315

316 **Author contributions**

317

318 L.L.P.-G. and R.B. conceived the project. All authors contributed to experimental
319 design, analysis and interpretation of results. Experimental contributions were as
320 follows: L.L.P.-G. (Fig. 2; Fig. 3e; Fig. 4a; ED Fig. 1); A.F.S. (Fig. 1d-f; Fig. 3e,f;
321 Fig. 4b-e; ED Fig. 1, ED Fig. 2c,e), M.A.K. (Fig. 5 and ED Fig. 3), S.C. (Fig.
322 3a,c,d and ED Fig. 2a-d). K.B. and S.P. performed RNA-seq data analysis. R.B.,
323 L.L.P.-G. and A.F.S. wrote the paper with input from all other authors.

324

325

326 **Methods**

327

328 ***Drosophila* culture**

329

330 Flies were maintained at 25°C in 12 h light:12 h dark conditions, except where
331 noted. *D. melanogaster* strains were cultured on a standard cornmeal diet; other
332 drosophilid species were grown on food sources as indicated in Extended Data
333 Table 4 (for recipes: <http://blogs.cornell.edu/drosophila/recipes>). Published
334 mutant and transgenic *D. melanogaster* are described in Extended Data Table 4.
335 *Df(3L)H99/Df(3L)XR38* (and their controls) were cultured at 22°C to increase the
336 number obtained of adult offspring of the desired genotype. For most histological
337 experiments, only female flies were analysed, to avoid confounding variation due
338 to known sexual dimorphisms²⁴. Mixed genders were used for
339 *Df(3L)H99/Df(3L)XR38* flies in Fig. 1d due to the limitation in the recovery of this
340 genotype, as well as for anti-IR75b and anti-IR75c immunofluorescence in Fig. 3e
341 (there is no sexual dimorphism in the numbers of these OSNs). For histological
342 experiments, flies were 1-12 days old. Animals subjected to antennal
343 deafferentation (and control intact flies) were left for 10 days post-surgery to
344 permit degeneration of OSN axons. For the experiments in Fig. 5 and Extended
345 Data Fig. 3, all experiments were carried out with 8-15 day old, mated female
346 flies.

347

348 **Histology and image analysis**

349

350 Whole mount antennal immunofluorescence and RNA fluorescent *in situ*
351 hybridisation were performed essentially as described³⁸. Whole mount brain
352 immunofluorescence was performed essentially as described³⁹. Primary and
353 secondary antibodies are listed in Extended Data Table 5. Sources and/or
354 construction details of templates for RNA probes are provided in Extended Data
355 Table 6. Imaging was performed on a Zeiss confocal microscope LSM710 or
356 LSM880 using a 40x oil immersion objective.

357 For automated counting of Elav-positive cell bodies, confocal stacks were
358 imported into Fiji⁴⁰ and passed through a median 3D filter of radius 1 in all
359 dimensions. Images were subsequently thresholded using the 3D iterative
360 thresholding plug-in⁴¹, and cells automatically counted using the 3D object
361 counter.

362 Analyses of OSN numbers expressing specific olfactory receptor genes,
363 and morphological differences of the antennal lobes of control and PCD-blocked
364 animals were performed by experimenters blind to the genotype, using
365 RandomNames.bat ([https://github.com/DavidOVM/File-Name-](https://github.com/DavidOVM/File-Name-Randomizer/blob/master/RandomNames.bat)
366 [Randomizer/blob/master/RandomNames.bat](https://github.com/DavidOVM/File-Name-Randomizer/blob/master/RandomNames.bat)) to encode image names.

367

368 **Electrophysiology**

369

370 Single-sensillum recordings were performed and analysed essentially as
371 described^{42,43}. at1 sensilla were identified based upon their morphology and
372 characteristic distal distribution on the antenna; they could also be clearly
373 distinguished from the only other trichoid sensillum class, at4, which houses three
374 OSNs (Extended Data Fig. 3 and data not shown). Chemical stimuli and solvents
375 are described in Extended Data Table 7. For the experiments in Fig. 2, neuron

376 activity was recorded for 10 s, starting 3 s before a stimulation period of 0.5 s. For
377 the experiments in Fig. 5 and Extended Data Fig. 3, neuron activity was recorded
378 for 6 s, starting 2 s before a stimulation period of 0.5 s. Traces were analysed by
379 sorting spike amplitudes in AutoSpike; representative traces presented in the
380 figures were further processed in Adobe Illustrator CS (Adobe systems, San
381 Jose, CA). Spontaneous neuron activity was quantified by counting spontaneous
382 spikes in a 10 s recording window. Stimulus-evoked activity was quantified by
383 counting spikes in a 0.5 s window during odour stimulation, and then subtracting
384 this count from a 0.5 s recording window just prior to stimulation. For the solvent-
385 corrected quantifications in Fig. 2d-e, the responses to solvent (paraffin oil) were
386 subtracted from the responses to the odour. In Fig. 2b, sensilla were classified as
387 having two neurons if two different spike amplitudes were automatically detected
388 and/or corrected responses to the fruit odour mix were above 20 Hz.

389 390 **RNA-sequencing and analysis**

391
392 Antennal RNA was extracted from three biological replicates of control (*peb-*
393 *Gal4/+;Or49a-GFP/+*) and PCD-blocked (*peb-Gal4/+;Or49a-GFP/UAS-p35*)
394 animals. (The increased numbers of neurons labelled by *Or49a-GFP* was noted
395 in preliminary studies and we therefore incorporated this transgene into the
396 genotypes used in these experiments as an internal control; see below). For each
397 pair of biological replicates, ~200 animals were grown under identical conditions
398 and RNA was extracted in parallel using 2-5 day old flies, as described⁹. RNA
399 quality was assessed on a Fragment Analyzer (Advanced Analytical
400 Technologies, Inc.); all RNAs had an RQN of 9.8-10. From 100 ng total RNA,
401 mRNA was isolated with the NEBNext Poly(A) mRNA Magnetic Isolation Module.
402 RNA-seq libraries were prepared from the mRNA using the NEBNext Ultra II
403 Directional RNA Library Prep Kit for Illumina (New England Biolabs). Cluster
404 generation was performed with the resulting libraries using the Illumina TruSeq
405 PE Cluster Kit v4 reagents and sequenced on the Illumina HiSeq 2500 using
406 TruSeq SBS Kit v4 reagents (Illumina). Sequencing data were demultiplexed
407 using the bcl2fastq Conversion Software (version 2.20, Illumina).

408 Purity-filtered reads were adapters- and quality-trimmed with Cutadapt
409 (version 1.8⁴⁴). Reads matching to ribosomal RNA sequences were removed with
410 fastq_screen (version 0.11.1). Remaining reads were further filtered for low
411 complexity with reaper (version 15-065)⁴⁵. Reads were aligned to the *Drosophila*
412 *melanogaster* BDGP6.92 genome using STAR (version 2.5.3a⁴⁶). The number of
413 read counts per gene locus was summarised with htseq-count (v. 0.9.1)⁴⁷ using
414 *Drosophila melanogaster*.BDGP6.92 gene annotation. The quality of the RNA-seq
415 data alignment was assessed using RSeQC (v. 2.3.7)⁴⁸.

416 Statistical analysis was performed for genes in R (version 3.5.3). Genes
417 with low counts were filtered out according to the rule of 1 count per million in at
418 least 1 sample. Library sizes were scaled using TMM normalisation (EdgeR
419 package version 3.24.3)⁴⁹ and log-transformed with limma cpm function (Limma
420 package version 3.38.3)⁵⁰.

421 Differential expression was computed with limma for paired samples by
422 fitting the 6 samples into a linear model and performing the comparison PCD-
423 blocked antennae versus controls. Comparison of read number for *GFP* (encoded
424 by the *Or49a-GFP* transgene) was performed by mapping reads to the *GFP*
425 sequence with Bowtie2⁵¹: control antennal RNA: 139±9.5 reads/sample (mean ±

426 standard deviation); PCD-blocked antennal RNA: 227±8.7 reads/sample.
427 Moderated t-test was used for the comparison on a subset of 83 expressed
428 *D. melanogaster* genes including: *Or*, *Ir* and *Gr* genes as well as the four pro-
429 apoptotic genes (*grim*, *rpr*, *hid* and *skl*). For multiple testing correction, the *p*-
430 values were adjusted by the Benjamini-Hochberg method, which controls the
431 false discovery rate⁵². The volcano plot was generated in R by plotting the
432 log₂(fold change PCD-blocked vs control) against the -log(p value). Data points
433 were shaded according to mean expression value across all samples.

434

435 **Phylogenetic analysis**

436

437 Phylogenetic analysis of drosophilid species was conducted using 6
438 housekeeping proteins, encompassing two nuclear loci (*Adh* and *Xdh*) and four
439 mitochondrial loci (*COI*, *COII*, *COIII* and *ND2*). Available amino acid sequences
440 from Uniprot (<https://www.uniprot.org>, accession numbers are listed in Extended
441 Data Table 8) of each species were concatenated in Geneious (v11.0.5). A
442 multiple sequence alignment of 2939 positions was generated using the MAFFT
443 (v7.309) tool with E-INS-I parameters and scoring matrix 200 PAM / K=2⁵³. The
444 final tree was reconstructed using a maximum likelihood approach with the
445 GTR+G+I model of nucleotide substitution and 1000 rate categories of sites in
446 FastTree (v2.1.5). The tree was visualised and processed in Geneious (v11.0.5).

447

448 **Statistics and reproducibility**

449

450 Statistical analyses and plotting were made in RStudio (v1.1.463 R Foundation
451 for Statistical Computing, Vienna, Austria, 2005; R-project-org), except for the
452 RNA-seq analyses (described above). For statistical analyses, normality was first
453 assessed on datasets using a Shapiro test. If both datasets were normally
454 distributed, a two-sided t-test was performed; otherwise, a Wilcoxon-rank sum
455 test was performed.

456

457 **Data availability**

458

459 All relevant data supporting the findings of this study are available from the
460 corresponding author on request. RNA-seq data are available in GEO (Accession
461 GSE128725).

462

463 **References**

464

- 465 1 Dekkers, M. P., Nikolettou, V. & Barde, Y. A. Cell biology in
466 neuroscience: Death of developing neurons: new insights and implications
467 for connectivity. *J Cell Biol* 203, 385-393, (2013).
- 468 2 Yamaguchi, Y. & Miura, M. Programmed cell death in neurodevelopment.
469 *Dev Cell* 32, 478-490, (2015).
- 470 3 Buss, R. R., Sun, W. & Oppenheim, R. W. Adaptive roles of programmed
471 cell death during nervous system development. *Annu. Rev. Neurosci.* 29,
472 1-35, (2006).
- 473 4 Pinto-Teixeira, F., Konstantinides, N. & Desplan, C. Programmed cell
474 death acts at different stages of *Drosophila* neurodevelopment to shape
475 the central nervous system. *FEBS Lett* 590, 2435-2453, (2016).

- 476 5 Liou, N. F. *et al.* Diverse populations of local interneurons integrate into the
477 *Drosophila* adult olfactory circuit. *Nat Commun* 9, 2232, (2018).
- 478 6 Hara, Y., Sudo, T., Togane, Y., Akagawa, H. & Tsujimura, H. Cell death in
479 neural precursor cells and neurons before neurite formation prevents the
480 emergence of abnormal neural structures in the *Drosophila* optic lobe.
481 *Dev. Biol.* 436, 28-41, (2018).
- 482 7 Sen, A., Kuruvilla, D., Pinto, L., Sarin, A. & Rodrigues, V. Programmed cell
483 death and context dependent activation of the EGF pathway regulate
484 gliogenesis in the *Drosophila* olfactory system. *Mech Dev* 121, 65-78,
485 (2004).
- 486 8 Endo, K., Aoki, T., Yoda, Y., Kimura, K. & Hama, C. Notch signal
487 organizes the *Drosophila* olfactory circuitry by diversifying the sensory
488 neuronal lineages. *Nat. Neurosci.* 10, 153-160, (2007).
- 489 9 Chai, P. C., Cruchet, S., Wigger, L. & Benton, R. Sensory neuron lineage
490 mapping and manipulation in the *Drosophila* olfactory system. *Nat*
491 *Commun* 10, 643, (2019).
- 492 10 Reddy, G. V., Gupta, B., Ray, K. & Rodrigues, V. Development of the
493 *Drosophila* olfactory sense organs utilizes cell-cell interactions as well as
494 lineage. *Development* 124, 703-712, (1997).
- 495 11 Han, Z., Boas, S. & Schroeder, N. E. Unexpected Variation in
496 Neuroanatomy among Diverse Nematode Species. *Frontiers in*
497 *Neuroanatomy* 9, 162, (2015).
- 498 12 Herculano-Houzel, S., Catania, K., Manger, P. R. & Kaas, J. H.
499 Mammalian Brains Are Made of These: A Dataset of the Numbers and
500 Densities of Neuronal and Nonneuronal Cells in the Brain of Glires,
501 Primates, Scandentia, Eulipotyphlans, Afrotherians and Artiodactyls, and
502 Their Relationship with Body Mass. *Brain Behav Evol* 86, 145-163, (2015).
- 503 13 Strausfeld, N. J., Sinakevitch, I., Brown, S. M. & Farris, S. M. Ground plan
504 of the insect mushroom body: functional and evolutionary implications. *J*
505 *Comp Neurol* 513, 265-291, (2009).
- 506 14 Fang, W. Q. & Yuste, R. Overproduction of Neurons Is Correlated with
507 Enhanced Cortical Ensembles and Increased Perceptual Discrimination.
508 *Cell Rep* 21, 381-392, (2017).
- 509 15 Wilsch-Brauninger, M., Florio, M. & Huttner, W. B. Neocortex expansion in
510 development and evolution - from cell biology to single genes. *Curr. Opin.*
511 *Neurobiol.* 39, 122-132, (2016).
- 512 16 Kuida, K. *et al.* Reduced apoptosis and cytochrome c-mediated caspase
513 activation in mice lacking caspase 9. *Cell* 94, 325-337, (1998).
- 514 17 Rogulja-Ortmann, A., Luer, K., Seibert, J., Rickert, C. & Technau, G. M.
515 Programmed cell death in the embryonic central nervous system of
516 *Drosophila melanogaster*. *Development* 134, 105-116, (2007).
- 517 18 Avery, L. & Horvitz, H. R. A cell that dies during wild-type *C. elegans*
518 development can function as a neuron in a *ced-3* mutant. *Cell* 51, 1071-
519 1078, (1987).
- 520 19 Shanbhag, S. R., Muller, B. & Steinbrecht, R. A. Atlas of olfactory organs
521 of *Drosophila melanogaster*. 1. Types, external organization, innervation
522 and distribution of olfactory sensilla. *Int J Insect Morphol Embryol* 28, 377-
523 397, (1999).
- 524 20 Rodrigues, V. & Hummel, T. Development of the *Drosophila* olfactory
525 system. *Adv Exp Med Biol* 628, 82-101, (2008).

- 526 21 Endo, K. *et al.* Chromatin modification of Notch targets in olfactory receptor
527 neuron diversification. *Nature Neuroscience* 15, 224-233, (2011).
- 528 22 Couto, A., Alenius, M. & Dickson, B. J. Molecular, anatomical, and
529 functional organization of the *Drosophila* olfactory system. *Curr Biol* 15,
530 1535-1547, (2005).
- 531 23 Benton, R., Vannice, K. S., Gomez-Diaz, C. & Vosshall, L. B. Variant
532 ionotropic glutamate receptors as chemosensory receptors in *Drosophila*.
533 *Cell* 136, 149-162, (2009).
- 534 24 Grabe, V. *et al.* Elucidating the Neuronal Architecture of Olfactory
535 Glomeruli in the *Drosophila* Antennal Lobe. *Cell Rep* 16, 3401-3413,
536 (2016).
- 537 25 Jefferis, G. S. & Hummel, T. Wiring specificity in the olfactory system.
538 *Semin Cell Dev Biol* 17, 50-65, (2006).
- 539 26 Lee, G. *et al.* Essential role of grim-led programmed cell death for the
540 establishment of corazonin-producing peptidergic nervous system during
541 embryogenesis and metamorphosis in *Drosophila melanogaster*. *Biology*
542 *open* 2, 283-294, (2013).
- 543 27 Sweeney, L. B. *et al.* Temporal target restriction of olfactory receptor
544 neurons by Semaphorin-1a/PlexinA-mediated axon-axon interactions.
545 *Neuron* 53, 185-200, (2007).
- 546 28 Hay, B. A., Wolff, T. & Rubin, G. M. Expression of baculovirus P35
547 prevents cell death in *Drosophila*. *Development* 120, 2121-2129, (1994).
- 548 29 Ha, T. S. & Smith, D. P. A pheromone receptor mediates 11-*cis*-vaccenyl
549 acetate-induced responses in *Drosophila*. *J Neurosci* 26, 8727-8733,
550 (2006).
- 551 30 Hallem, E. A., Ho, M. G. & Carlson, J. R. The molecular basis of odor
552 coding in the *Drosophila* antenna. *Cell* 117, 965-979, (2004).
- 553 31 Hallem, E. A. & Carlson, J. R. Coding of odors by a receptor repertoire.
554 *Cell* 125, 143-160, (2006).
- 555 32 Fishilevich, E. & Vosshall, L. B. Genetic and functional subdivision of the
556 *Drosophila* antennal lobe. *Curr Biol* 15, 1548-1553, (2005).
- 557 33 Wagh, D. A. *et al.* Bruchpilot, a protein with homology to ELKS/CAST, is
558 required for structural integrity and function of synaptic active zones in
559 *Drosophila*. *Neuron* 49, 833-844, (2006).
- 560 34 Stensmyr, M. C., Dekker, T. & Hansson, B. S. Evolution of the olfactory
561 code in the *Drosophila melanogaster* subgroup. *Proc Biol Sci* 270, 2333-
562 2340, (2003).
- 563 35 de Bruyne, M., Smart, R., Zammit, E. & Warr, C. G. Functional and
564 molecular evolution of olfactory neurons and receptors for aliphatic esters
565 across the *Drosophila* genus. *J. Comp. Physiol. A Neuroethol. Sens.*
566 *Neural Behav. Physiol.* 196, 97-109, (2010).
- 567 36 Prieto-Godino, L. L. *et al.* Evolution of acid-sensing olfactory circuits in
568 drosophilids. *Neuron* 93, 661-676 e666, (2017).
- 569 37 Pop, S. *et al.* The role of cell death in sculpting functional and adaptive
570 neural networks in flies. *submitted*, (2019).
- 571 38 Saina, M. & Benton, R. Visualizing olfactory receptor expression and
572 localization in *Drosophila*. *Methods in Molecular Biology* 1003, 211-228,
573 (2013).

- 574 39 Sanchez-Alcaniz, J. A., Zappia, G., Marion-Poll, F. & Benton, R. A
575 mechanosensory receptor required for food texture detection in
576 *Drosophila*. *Nat Commun* 8, 14192, (2017).
- 577 40 Schindelin, J. *et al.* Fiji: an open-source platform for biological-image
578 analysis. *Nat Methods* 9, 676-682, (2012).
- 579 41 Ollion, J., Cochenne, J., Loll, F., Escude, C. & Boudier, T. TANGO: a
580 generic tool for high-throughput 3D image analysis for studying nuclear
581 organization. *Bioinformatics* 29, 1840-1841, (2013).
- 582 42 Benton, R. & Dahanukar, A. Electrophysiological recording from
583 *Drosophila* olfactory sensilla. *Cold Spring Harb Protoc* 2011, 824-838,
584 (2011).
- 585 43 Olsson, S. B. & Hansson, B. S. Electroantennogram and single sensillum
586 recording in insect antennae. *Methods Mol Biol* 1068, 157-177, (2013).
- 587 44 Martin, M. Cutadapt removes adapter sequences from high-throughput
588 sequencing reads. *EMBnet.journal* 17, (2011).
- 589 45 Davis, M. P., van Dongen, S., Abreu-Goodger, C., Bartonicek, N. &
590 Enright, A. J. Kraken: a set of tools for quality control and analysis of high-
591 throughput sequence data. *Methods* 63, 41-49, (2013).
- 592 46 Dobin, A. *et al.* STAR: ultrafast universal RNA-seq aligner. *Bioinformatics*
593 29, 15-21, (2013).
- 594 47 Anders, S., Pyl, P. T. & Huber, W. HTSeq--a Python framework to work
595 with high-throughput sequencing data. *Bioinformatics* 31, 166-169, (2015).
- 596 48 Wang, L., Wang, S. & Li, W. RSeQC: quality control of RNA-seq
597 experiments. *Bioinformatics* 28, 2184-2185, (2012).
- 598 49 Robinson, M. D., McCarthy, D. J. & Smyth, G. K. edgeR: a Bioconductor
599 package for differential expression analysis of digital gene expression
600 data. *Bioinformatics* 26, 139-140, (2010).
- 601 50 Ritchie, M. E. *et al.* limma powers differential expression analyses for
602 RNA-sequencing and microarray studies. *Nucleic Acids Res.* 43, e47,
603 (2015).
- 604 51 Langmead, B. & Salzberg, S. L. Fast gapped-read alignment with Bowtie
605 2. *Nat Methods* 9, 357-359, (2012).
- 606 52 Benjamini, Y. & Hochberg, Y. Controlling the False Discovery Rate: A
607 Practical and Powerful Approach to Multiple Testing. *Journal of the Royal*
608 *Statistical Society. Series B (Methodological)* 57, 289-300, (1995).
- 609 53 Katoh, K. & Standley, D. M. MAFFT multiple sequence alignment software
610 version 7: improvements in performance and usability. *Mol. Biol. Evol.* 30,
611 772-780, (2013).
- 612 54 Dweck, H. K. *et al.* Pheromones mediating copulation and attraction in
613 *Drosophila*. *Proceedings of the National Academy of Sciences of the*
614 *United States of America* 112, E2829-2835, (2015).
- 615 55 Vosshall, L. B., Wong, A. M. & Axel, R. An olfactory sensory map in the fly
616 brain. *Cell* 102, 147-159, (2000).
- 617 56 Benton, R., Vannice, K. S. & Vosshall, L. B. An essential role for a CD36-
618 related receptor in pheromone detection in *Drosophila*. *Nature* 450, 289-
619 293, (2007).
- 620
- 621
- 622

623 Figure Legends

624

625 **Figure 1. Inhibition of developmental programmed cell death results in** 626 **increased neuron numbers in the antenna.**

627 **a**, Schematic of the *Drosophila* third antennal segment showing the different
628 sensory structures.

629 **b**, Schematic of the lineage of an antennal disc sensory organ precursor (SOP)
630 giving rise to a sensillum containing two neurons (illustrated on the right). The
631 expression of a subset of molecular markers is shown; Elav is expressed in only
632 three of four neural precursors; one of these (Naa) as well as the Elav-negative
633 cell (Nbb) are eliminated by PCD. The lineage is based upon data from^{8,9,21}.

634 **c**, Simplified schematic of the PCD pathway in *Drosophila*, highlighting the
635 elements relevant for this study. Several intermediate steps between the pro-
636 apoptotic proteins (Rpr, Grim, Hid and Skl) and the executioner caspases are not
637 shown.

638 **d**, Elav expression in whole-mount antennae from control (*Df(3L)H99/+*; the wild-
639 type chromosome here and in other genotypes was derived from a *w¹¹¹⁸* parent)
640 and PCD-deficient (*Df(3L)H99/Df(3L)XR38*) animals. Scale bar = 10 μ m. Right:
641 quantifications of antennal neuron numbers of the indicated genotypes, including
642 an additional control genotype (*Df(3L)XR38/+*). *** indicates $p = 0.0007216$ for
643 the comparison to *Df(3L)H99/+* and $p = 0.0013224$ for the comparison to
644 *Df(3L)XR38/+* (Wilcoxon-sum rank test, corrected for multiple comparisons using
645 a Bonferroni correction). In this and subsequent panels, individual data points are
646 shown, overlaid with boxes indicating the median and first and third quartile of the
647 data; whiskers showing the limits of the distribution.

648 **e**, Elav expression in whole-mount antennae from control (*peb-Gal4/+*) and PCD-
649 blocked (*peb-Gal4/+;UAS-miR(grim,rpr,hid)*) animals. Scale bar = 10 μ m. Right:
650 quantifications of neuron numbers of these genotypes. *** indicates $p =$
651 0.0024×10^{-4} (t-test).

652 **f**, Elav expression in whole-mount antennae from control (*peb-Gal4/+*) and PCD-
653 blocked (*peb-Gal4/+;UAS-p35/+*) animals. Scale bar = 10 μ m. Right:
654 quantifications of neuron numbers of these genotypes. * indicates $p = 0.024$ (t-
655 test).

656

657 **Figure 2. Undead olfactory sensory neurons are functional.**

658 **a**, Representative extracellular electrophysiology traces of spontaneous activity
659 from neurons in an at1 sensillum of control (*peb-Gal4/+*) and PCD-blocked (*peb-
660 Gal4/+;UAS-p35/+*) animals. Automatically-detected spikes (see Methods) from
661 the neuron expressing OR67d are shown in blue, and those of the additional,
662 undead neuron(s) in black, as schematised in the cartoon on the left (cells fated
663 to die are shown with dashed outlines).

664 **b**, Quantifications of the proportion of sensilla containing either one neuron (grey)
665 or two (or more) neurons (red) in control (*peb-Gal4/+*) and PCD-blocked (*peb-
666 Gal4/+;UAS-p35/+*) animals.

667 **c**, Quantifications of the spontaneous activity of the indicated neurons for the
668 control and PCD-blocked genotypes.

669 **d**, Representative electrophysiology traces from at1 sensillum recordings in
670 control (*peb-Gal4/+*) and PCD-blocked (*peb-Gal4/+;UAS-p35/+*) animals upon
671 stimulation with a 0.5 s pulse (black horizontal bar) of the pheromone *11-cis-*

672 vaccenyl acetate (cVA) (10^{-2} dilution (v/v) in paraffin oil) or a mix of fruit odours
673 (butyl acetate, ethyl butyrate, 2-heptanone, hexanol, isoamyl acetate, pentyl
674 acetate; each odour at 10^{-2} dilution (v/v) in paraffin oil). Automatically-detected
675 spikes from the neuron expressing OR67d are shown in blue, and those of the
676 undead neuron(s) in black.

677 **e**, Quantifications of odour-evoked responses to fruit odours (see Methods) in
678 control (*peb-Gal4/+*) and PCD-blocked (*peb-Gal4/+;UAS-p35/+*) animals.

679

680 **Figure 3. Undead neurons express a subset of olfactory receptor genes.**

681 **a**, Gene expression differences between control and PCD-blocked antennae. The
682 volcano plot shows the differential expression (on the x-axis) of *D. melanogaster*
683 *Or*, *Ir* and *Gr* gene transcripts (each gene represented by a dot), as well as the
684 four pro-apoptotic genes (*grim*, *rpr*, *hid* and *skt*; red labels), plotted against the
685 statistical significance (on the y-axis). The mean expression level of individual
686 genes across all samples is shown by the shading of the dot, as indicated by the
687 grey scale on the right (units: $\log_2(\text{counts per million})$). Only chemosensory genes
688 showing a >1.5-fold increase in PCD-blocked antennae are labelled: blue labels
689 indicate genes whose expression in the antenna has previously been
690 demonstrated by RNA *in situ* hybridisation; magenta and green labels indicate
691 receptors normally only expressed in the adult maxillary palps and larval dorsal
692 organ, respectively; black labels indicate receptors that are expressed in
693 gustatory organs. The horizontal dashed line indicates a false discovery rate
694 threshold of 5%. Data for all *Or*, *Ir* and *Gr* genes are provided in Extended Data
695 Table 2.

696 **b**, Schematic summarising the normal olfactory organ/sensillum expression
697 pattern of the subset of up-regulated *Or* genes that display co-expression in wild-
698 type neurons (colour-coded as in **a**; genes showing no changes in transcript
699 levels are labelled in grey).

700 **c**, Representative images of RNA FISH for the indicated *Or* genes in whole mount
701 antennae of control (*peb-Gal4/+*) and PCD-blocked (*peb-Gal4/+;UAS-p35/+*)
702 animals. Scale bar = 10 μm . Quantifications of neuron numbers are shown at the
703 bottom. *** indicates *Or19a* $p = 6.526 \times 10^{-05}$ (t-test), *Or42b* $p = 0.008486$ (t-test),
704 *Or65a* $p = 4.701 \times 10^{-06}$ (Wilcoxon-sum rank test), *Or43a* $p = 5.888 \times 10^{-07}$ (t-test)
705 (see also Extended Data Fig. 2a). The pink dashed line encircles those cells in
706 the PCD-blocked antenna that express the corresponding *Ors* outside their usual
707 spatial domain (see also Extended Data Fig. 2b).

708 **d**, Representative images of RNA FISH for the indicated *Or* genes in whole
709 mount antennae of control (*peb-Gal4/+*) and PCD-blocked (*peb-Gal4/+;UAS-*
710 *p35/+*) animals. Scale bar = 10 μm . Quantifications of neuron numbers are shown
711 at the bottom. *** indicates *Or33a* $p = 1.812 \times 10^{-07}$ (t-test), *Or85e* $p = 0.053$
712 (Wilcoxon-sum rank test).

713 **e**, Representative images of immunohistochemistry or RNA FISH for the indicated
714 olfactory receptors in whole mount antennae of control (*peb-Gal4/+*) and PCD-
715 blocked (*peb-Gal4/+;UAS-p35/+*) animals. Scale bar = 10 μm . Quantifications of
716 neuron numbers are shown at the bottom. *, ns, and *** indicate, respectively,
717 IR75c $p = 0.01$ (t-test), IR75b $p = 0.9246$ (t-test), *Or22a* $p = 0.0002472$ (t-test).

718 **f**, Representative images of anti-GFP and RNA FISH for *Or85f* in whole mount
719 antennae of control (*peb-Gal4/+;Or49a-GFP/+*) and PCD-blocked (*peb-*
720 *Gal4/+;Or49a-GFP/UAS-p35*) animals. Scale bar = 10 μm . Quantifications of
721 neuron numbers are shown at the bottom. *** indicates *Or49a-GFP* $p = 1.444 \times 10^{-}$

722 ¹² (t-test), *Or85f* $p = 0.01375$ (t-test), merged panel *Or49a-GFP*⁺/*Or85f* mRNA
723 population $p = 5.48 \times 10^{-12}$ (t-test). The pink dashed line encircles those cells in the
724 PCD-blocked antenna that express *Or49a-GFP* outside its usual spatial domain.
725 We used an *Or49a-GFP* reporter, due to our inability to reliably detect *Or49a*
726 transcripts *in situ*; the higher number of *Or49a-CD8:GFP*-positive *Or85f* RNA-
727 positive cells is not an artefact of the analysis method, as an *Or85f-CD8:GFP*
728 reporter revealed a similarly limited increase in neuron number (Extended Data
729 Fig. 2e).

730

731 **Figure 4. Undead olfactory sensory neurons form novel wiring properties in**
732 **the brain.**

733 **a**, Representative images of anti-GFP immunofluorescence in whole mount
734 antennae of control (*peb-Gal4/+; grim^{MI03811(EGFP)/+}*) and PCD-blocked (*peb-*
735 *Gal4/+; UAS-p35/+; grim^{MI03811(EGFP)/+}*) animals. Blind scoring by two independent
736 observers of antennae as belonging to control or PCD-blocked group was 100%
737 accurate (see methods). Scale bar = 10 μm .

738 **b**, Representative images of combined anti-GFP and nc82 immunofluorescence
739 in whole mount brains of control (*peb-Gal4/+; grim^{MI03811(EGFP)/+}*) and PCD-
740 blocked (*peb-Gal4/+; UAS-p35/+; grim^{MI03811(EGFP)/+}*) animals with intact (left) or
741 excised antennae (right). Blind categorisation of brains ($n = 9-12$ brains per
742 genotype) as belonging to the control or PCD-blocked set was 95% accurate (2
743 independent observers). Scale bar = 10 μm .

744 **c**, Representative images of combined anti-GFP and nc82 immunofluorescence
745 in whole mount brains of control (*peb-Gal4/+; Or49a-GFP/Or49a-GFP; GH146-*
746 *QF, QUAS-Tomato/+*) and PCD-blocked (*peb-Gal4/+; Or49a-GFP/Or49a-*
747 *GFP, UAS-p35; GH146-QF, QUAS-Tomato/+*) animals. Blind categorisation of
748 brains ($n = 9$ and 7 brains, respectively, per genotype) as belonging to the control
749 or PCD-blocked group was 100% accurate (1 observer). Scale bar = 10 μm .

750 **d**, Representative images of combined anti-GFP, anti-RFP and nc82
751 immunofluorescence in whole mount brains of control (*peb-Gal4/+; Or49a-*
752 *GFP/Or49a-GFP; GH146-QF, QUAS-Tomato/+*) and PCD-blocked (*peb-*
753 *Gal4/+; Or49a-GFP/Or49a-GFP, UAS-p35; GH146-QF, QUAS-Tomato/+*) animals.
754 Scale bar = 10 μm .

755 **e**, Representative images of PN soma (bounded by the dashed lines) labelled by
756 *GH146>Tomato* in whole mount brains of control (*peb-Gal4/+; Or49a-GFP/*
757 *Or49a-GFP; GH146-QF, QUAS-Tomato/+*) and PCD-blocked (*peb-Gal4/+; Or49a-*
758 *GFP/Or49a-GFP, UAS-p35; GH146-QF, QUAS-Tomato/+*) animals. Scale bar = 10
759 μm . Quantifications of neuron numbers are shown to the right. *ns* indicates $p =$
760 0.819 (t-test).

761

762 **Figure 5. Examples of naturally occurring extra neurons in at1 sensilla.**

763 **a**, Representative traces of extracellular recordings of neuronal responses to a
764 0.5 s pulse (black horizontal bar) of solvent (dichloromethane) or cVA in *D.*
765 *melanogaster* and *D. subobscura* ($n = 5$). A single cVA-responsive neuron
766 (known or assumed to express OR67d orthologues) is detected (blue spikes), as
767 schematised in the cartoon on the left.

768 **b**, Representative traces of extracellular recordings of neuronal responses to a
769 0.5 s pulse (black horizontal bar) of solvent (dichloromethane) or cVA in *D.*
770 *nasuta*, *D. pallidipennis* and *D. testacea* ($n = 3-5$). Two spike amplitudes are
771 detected: a cVA-responsive neuron (assumed to express OR67d orthologues)

772 (blue spikes) and second neuron with a larger spike amplitude, which does not
773 respond to cVA (black spikes), as schematised in the cartoon on the left.
774 **c**, Phylogeny of 24 drosophilid species, representing the majority of
775 the *Drosophila* genus subgroups, based on the protein sequences of
776 housekeeping loci (see Methods). Species names are coloured to reflect the
777 presence of one or two neurons in at1 sensilla. Numbers next to the tree nodes
778 indicate the support values. The scale bar for branch length represents the
779 number of substitutions per site.

780

781 **Extended Data**

782 **Extended Data Figure 1. Automated quantification of Elav-positive olfactory** 783 **sensory neurons.**

784 Representative example of Elav expression in whole-mount antennae from
785 control (*peb-Gal4/+*) and PCD-blocked (*peb-Gal4/+;UAS-p35/+*) animals. Middle:
786 output of automated image segmentation of the same antennae used for
787 quantification of OSN number (see Methods). Right: overlay of both images.
788 Scale bar = 10 μ m.

789

790 **Extended Data Figure 2. Characterisation of Or expression in PCD-blocked** 791 **antennae.**

792 **a**, Representative images of RNA FISH for *Or69a* in whole mount antennae of
793 control (*peb-Gal4/+*) and PCD-blocked (*peb-Gal4/+;UAS-p35/+*) animals. Scale
794 bar = 10 μ m. Quantifications of neuron numbers are shown at the bottom. ***
795 indicates $p = 1.811 \times 10^{-05}$ (Wilcoxon-sum rank test).

796 **b**, Additional representative images of RNA FISH for *Or19a* and *Or43a* in whole
797 mount antennae of control (*peb-Gal4/+*) and PCD-blocked (*peb-Gal4/+;UAS-*
798 *p35/+*) animals. Scale bar = 10 μ m. The pink dashed line encircles those cells in
799 the PCD-blocked antenna that express *Ors* outside their usual spatial domain.

800 **c**, Representative images of RNA FISH for the indicated *Or* genes in whole mount
801 antennae of control (*peb-Gal4/+*) and PCD-blocked (*peb-Gal4/+;UAS-p35/+*)
802 animals. Quantifications of neuron numbers are shown at the bottom. Scale bar =
803 10 μ m. *ns* indicates *Or13a* $p = 0.4759$, *Or35a* $p = 0.7132$ (t-test), *Or67d* $p =$
804 0.05341 (Wilcoxon-sum rank test).

805 **d**, Representative images of combined RNA FISH for *Or65a* (green) and *Or65b*
806 (magenta) in whole mount antennae of control (*peb-Gal4/+*) and PCD-blocked
807 (*peb-Gal4/+;UAS-p35/+*) animals, showing co-expression of these receptors in
808 both endogenous and undead neurons. Scale bar = 10 μ m.

809 **e**, Representative images of RNA FISH for *Or85f* and anti-GFP in whole mount
810 antennae of control (*peb-Gal4/+;Or85f-GFP/+*) and PCD-blocked (*peb-*
811 *Gal4/+;Or85f-GFP/UAS-p35*) animals. Scale bar = 10 μ m. Quantifications of
812 neuron numbers are shown at the bottom. * indicates *Or85f* mRNA $p = 0.01375$
813 (t-test), GFP $p = 0.0153$ (t-test).

814

815 **Extended Data Figure 3. Electrophysiological distinction of at1 and at4** 816 **sensilla.**

817 Representative traces of extracellular recordings of neuronal responses to a 0.5 s
818 pulse (black horizontal bar) of methyl laurate (diluted 1:10 v/v), cVA (1:10) or
819 solvent (dichloromethane) in at1 or at4 sensilla of *D. melanogaster* and *D.*
820 *testacea* ($n = 5$). Methyl laurate permits functional distinction of these sensillum

821 classes, as it does not activate the Or67d neuron in *D. melanogaster*, or either
822 neuron in the 2-neuron at1 sensilla of *D. testacea*; by contrast, this pheromone
823 robustly activates at4 sensilla neurons (corresponding to the Or47b and Or88a
824 neuron classes in *D. melanogaster*⁵⁴).

825

826 **Extended Data Table 1. Estimated potential pool of undead neurons in the**
827 **antenna.**

828 The number of potential undead neurons in the antenna was calculated from
829 information on the number of each neuron/sensillum class and the number of
830 neurons that are normally removed by PCD. Estimations of neuron numbers are
831 taken from quantification of *Or*- and *Ir-Gal4* driver expression²⁴, except where
832 direct analysis of receptor gene expression is available (by RNA FISH or
833 immunofluorescence, as indicated in the Notes column). As the numbers of
834 neurons for the classes housed in the same sensillum should be identical – but
835 may vary due to technical reasons – the mean of the individual values was
836 calculated to provide a more accurate estimation of the number of each sensillum
837 type, and thereby the total number of antennal neurons; these are largely
838 concordant with previous estimates¹⁹. The “# potential undead neurons/sensillum”
839 values are based on the assumption that only three of four potential OSNs
840 express Elav during development²¹ (except in ab1 where there are four Elav-
841 positive cells); thus, sensilla that house one, two or three neurons, could
842 potentially give rise to two, one or zero additional undead Elav-positive cells if
843 PCD is blocked.

844 *Provided as an accompanying Excel file.*

845

846 **Extended Data Table 2. Comparison of chemosensory receptor and pro-**
847 **apoptotic factor transcript abundance in control and PCD-blocked antennae.**

848 *Provided as an accompanying Excel file.*

849

850 **Extended Data Table 3. *In situ* expression properties of chemosensory**
851 **genes up-regulated in PCD-blocked antennae.**

852 The chemosensory genes listed are the subset displaying a >1.5-fold increase in
853 expression in PCD-blocked antennae compared to control antennae from
854 Extended Data Table 2. *In situ* expression data are derived from previous
855 studies^{9,21-23,32}; sensilla name abbreviations are shown in Extended Data Table 1
856 (pb = maxillary palp basiconic).

857 *Provided as an accompanying Excel file.*

858

859 **Extended Data Table 4. Drosophilid stocks.**

860

Genotype	Source	Reference
<i>w</i> ¹¹¹⁸		
<i>peb-Gal4</i>	L. Luo	27
<i>UAS-p35</i>	BDSC	BL-5072
<i>UAS-miR(grim,rpr,hid)</i>	D. Williams	26
<i>Df(3L)H99</i>	BDSC	BL-1576
<i>Df(3L)XR38</i>	BDSC	BL-2099
<i>Mi{MIC}grim</i> ^{M103811}	BDSC	BL-36978
<i>Or49a-CD8:GFP</i>	BDSC	BL-52629
<i>Or85f-CD8:GFP</i>	BDSC	BL-52643

<i>GH146-QF</i>	BDSC	BL-30015
<i>QUAS-Tomato</i>	BDSC	BL-30005
<i>D. affinis</i> (banana)	DSSC	14012□0141.00
<i>D. busckii</i> (banana)	DSSC	13000□0081.00
<i>D. cardini</i> (banana)	DSSC	1518□2181.03
<i>D. erecta</i> (cornmeal)	DSSC	14021□0224.01
<i>D. ficusphila</i> (banana)	DSSC	14025□0441.01
<i>D. hamatofila</i> (banana)	DSSC	15081□1301.05
<i>D. immigrans</i> (cornmeal)	DSSC	15111□1731.10
<i>D. macrospina</i> (banana)	DSSC	15120□1931.00
<i>D. mauritiana</i> (banana)	DSSC	14021□0241.150
<i>D. melanogaster</i> CS (cornmeal)		
<i>D. nanoptera</i> (banana)	DSSC	15090□1692.00
<i>D. nasuta</i> (cornmeal)	DSSC	15112□178.01
<i>D. nebulosa</i> (cornmeal)	DSSC	14030□0761.00
<i>D. neocordata</i> (banana)	DSSC	14041□0831.00
<i>D. pallidipennis</i> (banana)	DSSC	15210□2331.02
<i>D. pseudoobscura</i> (banana)	DSSC	14011□0121.00
<i>D. putrida</i> (banana)	DSSC	15150□2101.00
<i>D. repletoides</i> (banana)	DSSC	15250□2451.01
<i>D. sechellia</i> (cornmeal/noni juice)	DSSC	14021□0248.07
<i>D. simulans</i> (cornmeal)	DSSC	14021□0251.01
<i>D. subobscura</i> (banana)	DSSC	14011□0131.04
<i>D. takahashii</i> (cornmeal/blueberry)	DSSC	14022□0311.00
<i>D. testacea</i> (banana)	DSSC	15150□2101.00
<i>D. yakuba</i> (cornmeal)	DSSC	14021□0261.40

861
862
863

Extended Data Table 5. Antibodies.

Antibody	Dilution	Source/Reference
Mouse anti-Elav	1:10	DSHB
Rabbit anti-RFP	1:250	Abcam ab62341
Chicken anti-GFP	1:1000	Abcam ab13970
Rabbit anti-IR75b	1:100	³⁶
Guinea pig anti-IR75c	1:100	³⁶
Mouse anti-Bruchpilot (nc82)	1:10	DSHB

864
865
866

Extended Data Table 6. Template construction for RNA FISH probes.

RNA probe	Forward / reverse primers (5'-3')	Source
<i>Or19a</i>		²²
<i>Or22a</i>		⁵⁵
<i>Or33b</i>		²²

<i>Or42b</i>		9
<i>Or43a</i>	CCGGTGA CTGCGATGAATCT / CTCGTACCAGGGCACATTGT	<i>This work</i>
<i>Or47a</i>		55
<i>Or49a</i>		22
<i>Or65a</i>		22
<i>Or65b</i>		22
<i>Or67a</i>		56
<i>Or69a</i>		55
<i>Or85e</i>		55
<i>Or85f</i>	ATGGAACCTGTGCAGTACAG / CTACTGAATCATCTGCATGAGCA	<i>This work</i>

867
868
869

Extended Data Table 7. Chemical stimuli.

Chemical	Source	CAS
<i>11-cis-vaccenyl acetate</i>	Pherobank (Fig. 2); AKos Consulting Solutions (Fig. 5, Extended Data Fig. 3)	6186-98-7
butyl acetate	Sigma-Aldrich	123-86-4
ethyl butyrate	Sigma-Aldrich	105-54-4
2-heptanone	Sigma-Aldrich	110-43-0
hexanol	Sigma-Aldrich	111-27-3
isoamyl acetate	Sigma-Aldrich	123-92-2
pentyl acetate	Sigma-Aldrich	628-63-7
methyl laurate	Sigma-Aldrich	111-82-0
dichloromethane	Sigma-Aldrich	75-09-2
paraffin oil	Sigma-Aldrich	8012-95-1

870
871
872
873
874
875
876

Extended Data Table 8. Accession numbers of the housekeeping protein sequences used to reconstruct the drosophilid phylogenetic tree.

Provided as an accompanying Excel file.

Figure 1

bioRxiv preprint doi: <https://doi.org/10.1101/623488>; this version posted May 2, 2019. The copyright holder for this preprint (which was not certified by peer review) is the author/funder. All rights reserved. No reuse allowed without permission.

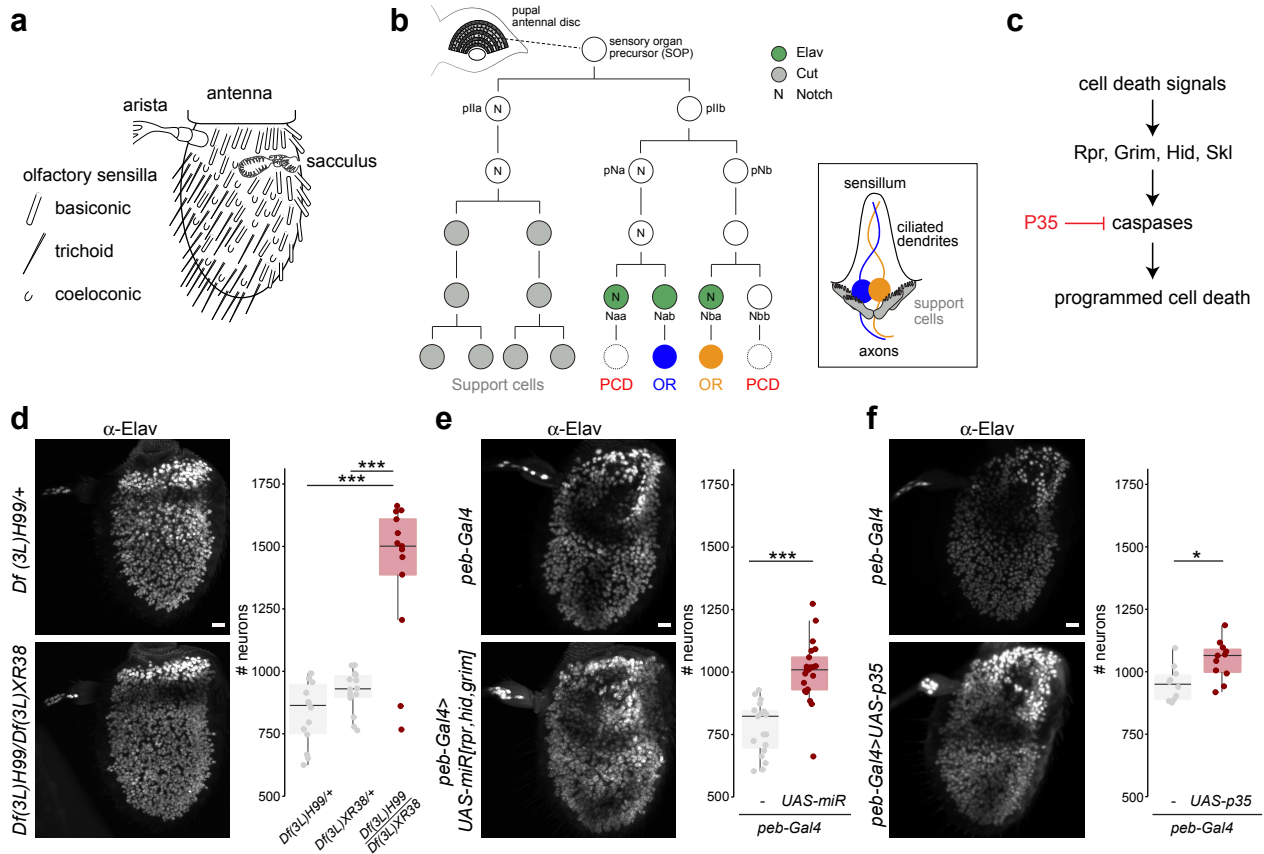


Figure 2

bioRxiv preprint doi: <https://doi.org/10.1101/623488>; this version posted May 2, 2019. The copyright holder for this preprint (which was not certified by peer review) is the author/funder. All rights reserved. No reuse allowed without permission.

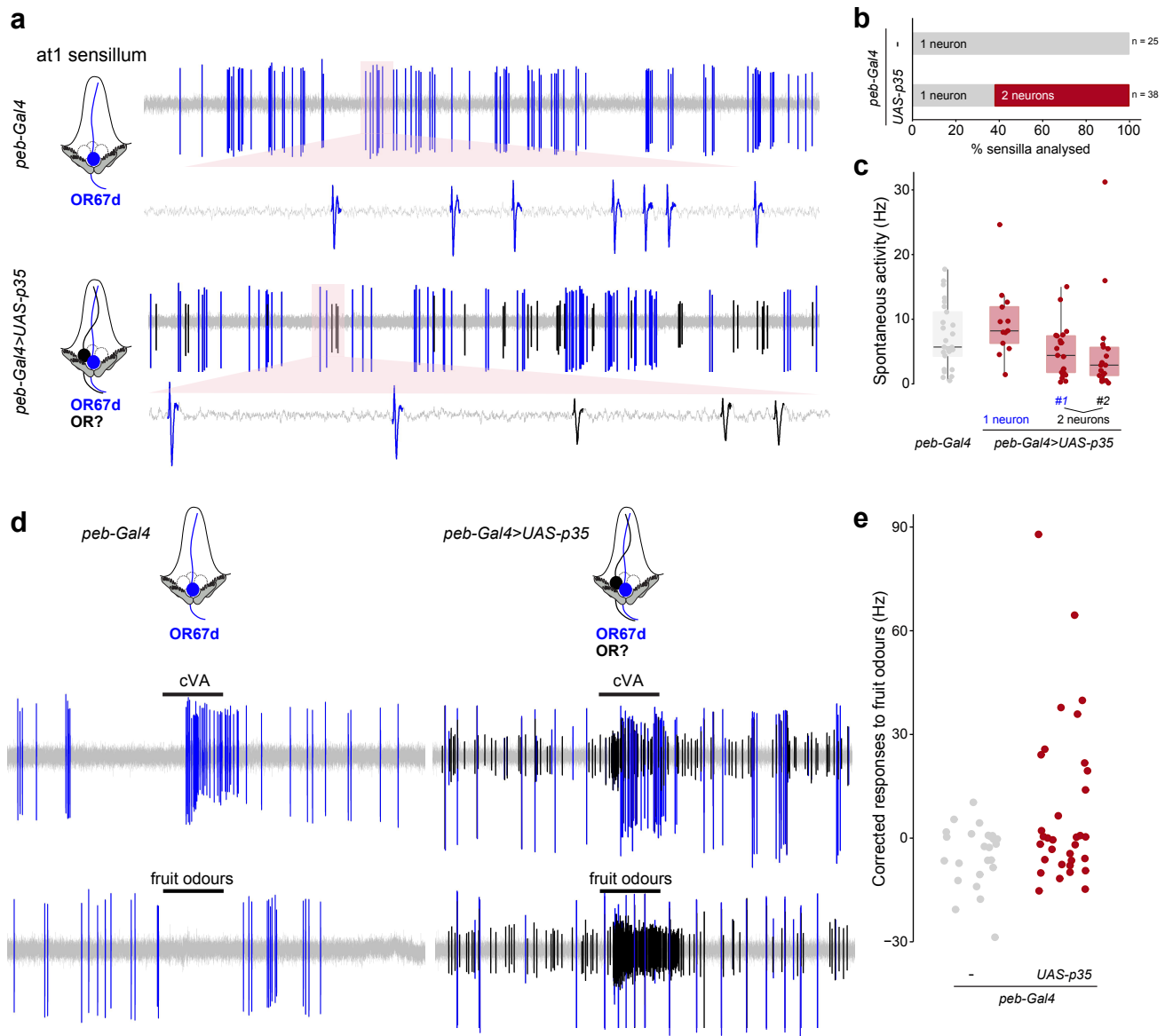


Figure 3

bioRxiv preprint doi: <https://doi.org/10.1101/623488>; this version posted May 2, 2019. The copyright holder for this preprint (which was not certified by peer review) is the author/funder. All rights reserved. No reuse allowed without permission.

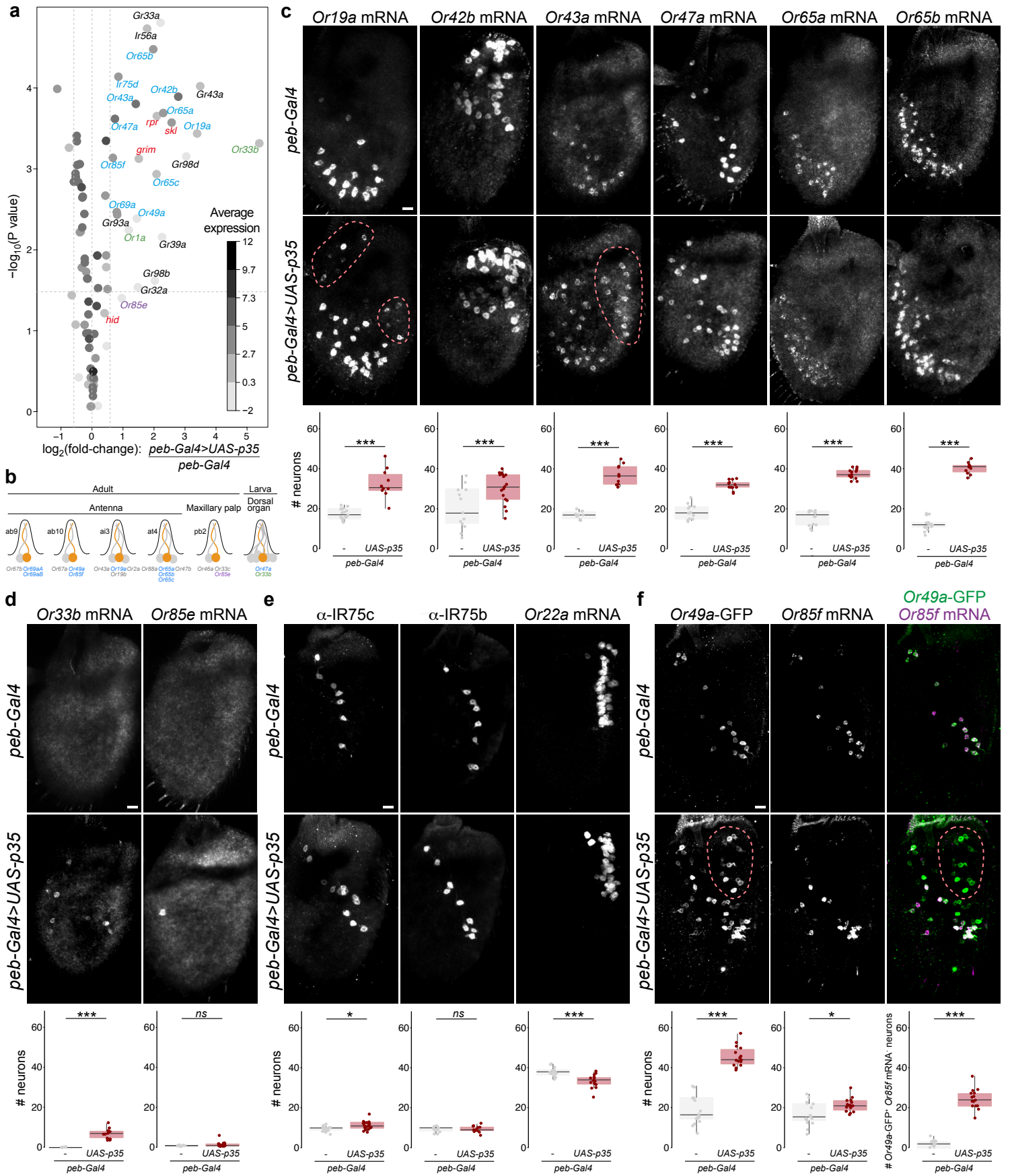


Figure 4

bioRxiv preprint doi: <https://doi.org/10.1101/623488>; this version posted May 2, 2019. The copyright holder for this preprint (which was not certified by peer review) is the author/funder. All rights reserved. No reuse allowed without permission.

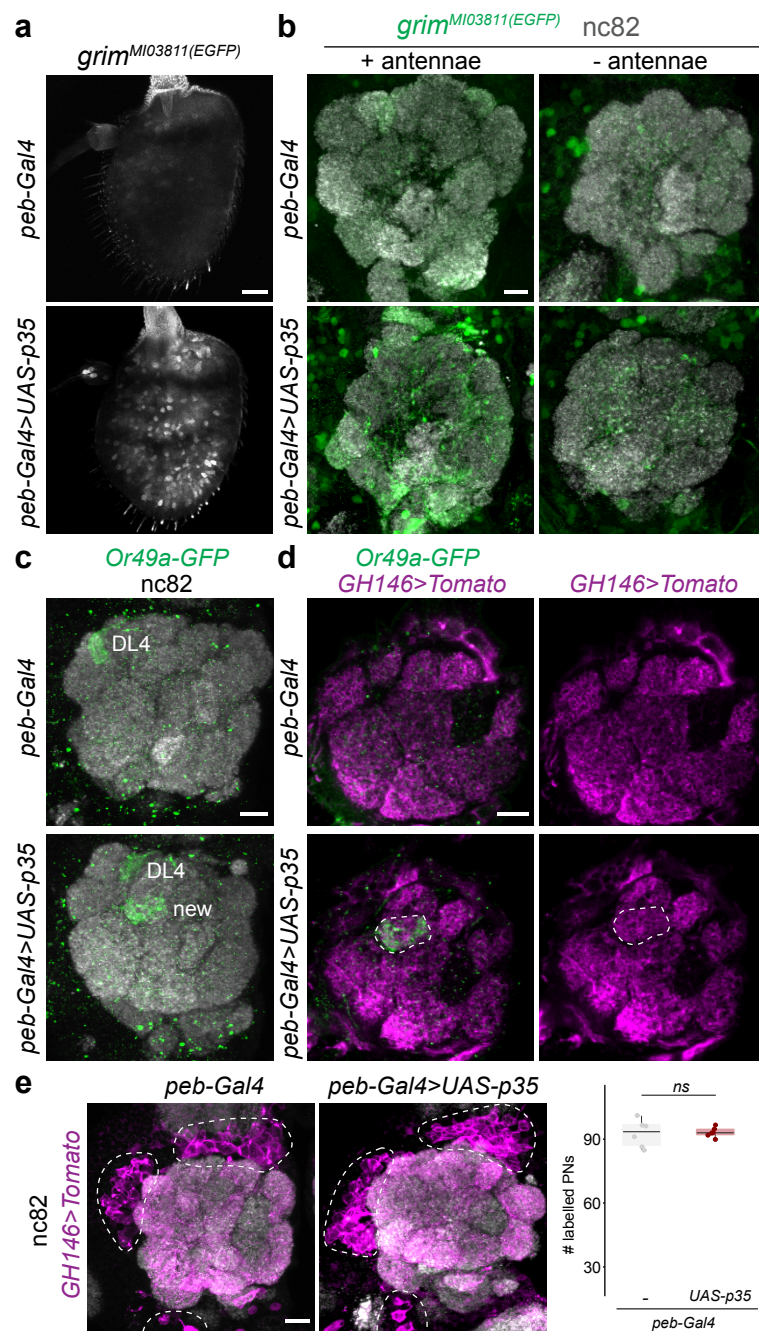
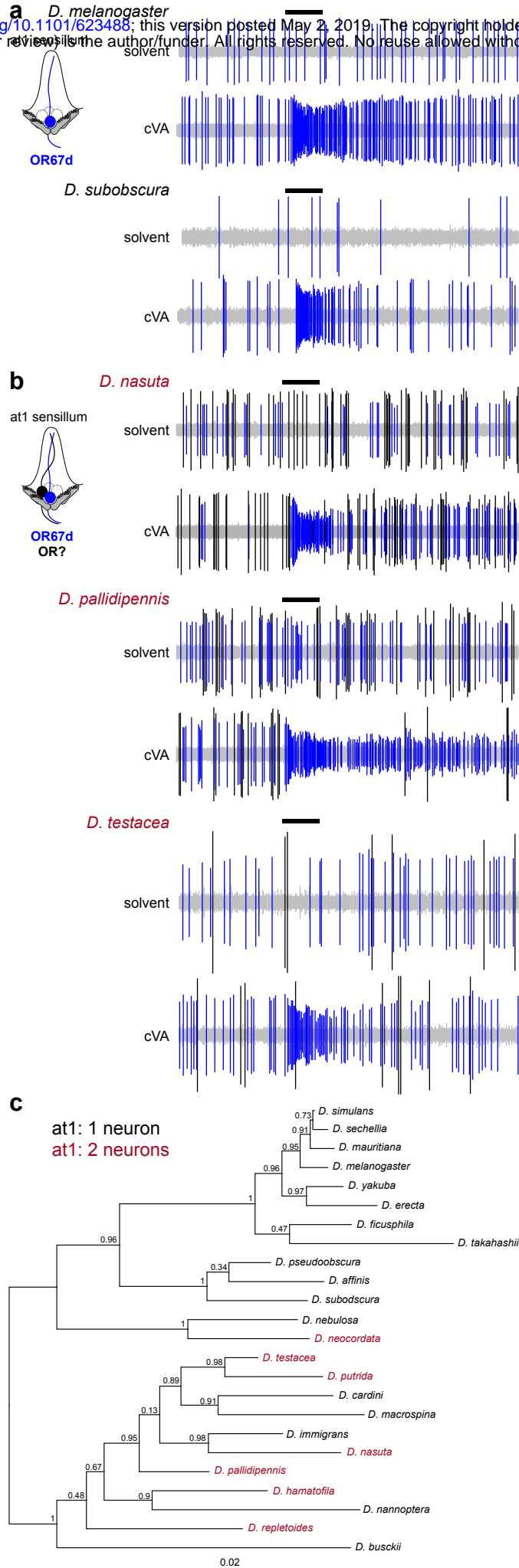


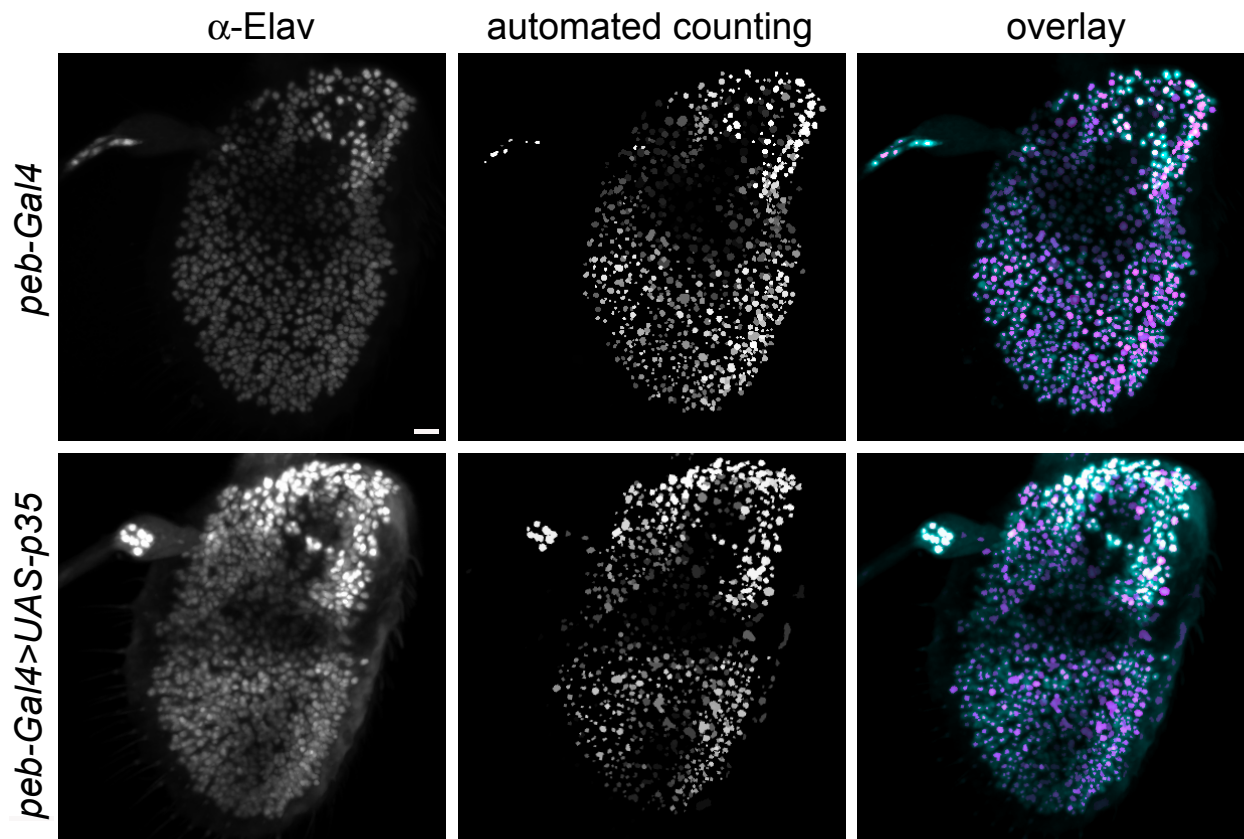
Figure 5

bioRxiv preprint doi: <https://doi.org/10.1101/623488>; this version posted May 2, 2019. The copyright holder for this preprint (which was not certified by peer review) is the author/funder. All rights reserved. No reuse allowed without permission.



Extended Data Figure 1

bioRxiv preprint doi: <https://doi.org/10.1101/623488>; this version posted May 2, 2019. The copyright holder for this preprint (which was not certified by peer review) is the author/funder. All rights reserved. No reuse allowed without permission.



Extended Data Figure 3

bioRxiv preprint doi: <https://doi.org/10.1101/623488>; this version posted May 2, 2019. The copyright holder for this preprint (which was not certified by peer review) is the author/funder. All rights reserved. No reuse allowed without permission.

